Decoding entangled transitions: Polyamorphism and stressed rigidity

Can Yildirim, Jean-Yves Raty, and Matthieu Micoulaut

Citation: The Journal of Chemical Physics **148**, 244505 (2018); doi: 10.1063/1.5034500
View online: https://doi.org/10.1063/1.5034500
View Table of Contents: http://aip.scitation.org/toc/jcp/148/24
Published by the American Institute of Physics

PHYSICS TODAY
WHITEPAPERS

ADVANCED LIGHT CURE ADHESIVES

Take a closer look at what these environmentally friendly adhesive systems can do

READ NOW

PRESENTED BY
MASTERBOND
ADHESIVES | SEALANTS | COATINGS

Decoding entangled transitions: Polyamorphism and stressed rigidity

Can Yildirim,[1,2,3] Jean-Yves Raty,[2] and Matthieu Micoulaut[1,a)]
[1]*Laboratoire de Physique Théorique de la Matière Condensée, Sorbonne Université, 4 Place Jussieu, 75252 Paris Cedex 05, France*
[2]*Physique de la Matière Condensée, B5, Université de Liège, B4000 Sart-Tilman, Belgium*
[3]*European Synchrotron Radiation Facility, 71, Avenue des Martyrs, CS 40220, 38043 Grenoble Cedex 9, France*

(Received 12 April 2018; accepted 5 June 2018; published online 26 June 2018)

There is much to learn from simulation studies of polyamorphism achieved for systems with different bonding environments. Chalcogenide glasses such as Ge–Se glasses undergo an elastic phase transition involving important changes in network connectivity. Stimulated by recent developments of topological constraint theory, we show that the concept of rigidity can be extended to a broader range of thermodynamic conditions including densified glasses. After having validated our structural first principles molecular dynamics models with experimental data over a broad pressure range for $GeSe_4$, we show that the onset of polyamorphism is strongly related to the constraint density measuring the degree of rigidity of the network backbone, while voids and cavities in the structure collapse at very small pressures. This leads to the identification that the progressive onset of higher coordinated species typical of high pressure phases is responsible for the onset of stressed rigidity, although the constraint analysis also indicates progressive stiffening of bonding angles. Results are compared to stoichiometric and stressed rigid $GeSe_2$ and to isostatic As_2Se_3 and then generalized to other compositions in the Ge–Se binary under pressure. *Published by AIP Publishing.* https://doi.org/10.1063/1.5034500

I. INTRODUCTION

Although they differ from crystals due to a lack of translational periodicity and long-range order at the atomic scale, amorphous materials bear with crystals the ability to exist in different forms, a feature known as polyamorphism.[1] It is now widely recognized that the manifestation of such basic phenomena, driven by applied pressure, results from different atomic coordinations and structures that can lead to amorphous phases of the same chemical composition but with different physical properties. The question whether polyamorphism involves a phase transition between two distinct metastable amorphous states remains an actively debated topic,[2] and it is still not clear if the observed low temperature polyamorphic transition is an extension of the reported liquid-liquid transition between two stable liquid states.

Besides the archetypal example of amorphous ice[3] which can be found in at least two amorphous phases, low density (LDA) and high density (HDA), a certain number of other materials have been found to display such transformations including carbon, silicon, germanium,[4] or yttria-alumina alloys.[2] Oxide glasses such as silica[5] or germania[6] have been also investigated in this context, and both simulation and diffraction results have shown that the application of pressure transforms the basic tetrahedral structure into a network of predominantly octahedral nature, typical of high pressure crystalline polymorphs, as, e.g., stishovite. To our knowledge, the same aspects in corresponding chalcogenides have received much less attention,[7] although very recent studies have emphasized that these tetrahedral to octahedral conversions occur as well.[8–10] However, the transformations appear to be more complicated due to the covalent nature of the bonding and to a more complex network connectivity made of both corner-sharing (CS) and edge-sharing (ES) tetrahedra.[11]

Here we decode the intrinsic connection between polyamorphism and molecular rigidity, the latter capturing the aspects of topology which contribute to the stiffening of an atomic network, identified as a mechanical truss and characterized by a constraint density (n_c) due to molecular interactions. This approach shows that an elastic rigidity transition can be achieved between a flexible phase with low connectivity ($n_c < 3$) and a stressed rigid phase which is overconstrained[11] ($n_c > 3$).

Using First Principles Molecular Dynamics (FPMD) simulations and topological constraint algorithms,[12] we show, indeed, that as pressure is applied to $GeSe_4$, a clear threshold at ≃10 GPa separating LDA and HDA phases is obtained in agreement with reported experiments[8] but within a pressure range (0–50 GPa) that now permits a full characterization of the HDA phase and a neat detection of the pressure range at which the network structure evolves markedly between LDA and HDA. The reasons for choosing $GeSe_4$ are motivated by (i) an abundant experimental database allowing for multiple validations of the pressurized structural models and (ii) the fact that the glass is isostatic and fulfills exactly $n_c = 3$. The detailed atomic scale and the topological constraint analyses then show that a substantial increase of the constraint density n_c occurs in the vicinity of the LDA-HDA transformation, the increase of topological constraints being identified with the onset of

a)Author to whom correspondence should be addressed: mmi@lptmc.jussieu.fr

stressed rigidity, once a dramatic reduction of voids and cavities at small pressures has been achieved. A comparison with other simulated systems permits us to consider the effect of pressure on a stressed rigid glass ($GeSe_2$) and another isostatic one (As_2Se_3). A general increase of topological constraints is acknowledged for all the considered systems, the effect of pressure on stressed rigid networks leading to exceptionally large rigidity levels at moderate pressures (20 GPa). The transformation is also characterized by a rapid evolution of the Se–Se and Ge–Se bond statistics with pressure. While previous connections have been made between rigidity and pressure induced transformations in oxides,[13] here it is the first time that such transformations, polyamorphic or stiffness, are investigated simultaneously, fully characterized, and contrasted. While the LDA-HDA transformation is obviously correlated with a coordination number increase $r(P)$ as previously reported,[5,8] the present results provide a more complex picture in which a pressure induced stiffening of angular motion is also evidenced. Having such detailed information in hand, we finally generalize the findings and provide a link between the LDA-HDA transformation pressures and network connectivity in densified Ge–Se glasses and in other glass-forming systems.

II. NUMERICAL METHODS

We used *ab initio* molecular dynamics (AIMD) to model the structural modifications in $GeSe_4$ for various pressures. As embedded in the Car-Parrinello molecular dynamics (CPMD) code, we have utilized a density functional theory (DFT) scheme to describe the electronic structure that evolves self-consistently with time. For exchange correlation energies, the Becke, Lee, Yang, and Parr approach[11] in conjunction with a generalized gradient approximation was used. The Troullier-Martins type pseudopotential approximation was adopted. Our simulations were carried out in an NVT ensemble, i.e., the number of atoms, volume, and temperature of the system were kept constant with a total of 250 atoms. The cell dimensions were determined according to the experimental densities available in the literature[14] or to their extrapolations.[15] The initial positions of the atoms were taken from the GeSe crystal, and Ge atoms are replaced with Se atoms to reach the target composition. The wavefunctions have been expanded at the Γ point of the supercell on a plane-wave basis set having a cut-off energy of 20 Ry. A time step of Δt = 0.1 fs was used to the integrate equations of motion using the Verlet algorithm. The fictitious electron mass was selected as 200 a.u. The initial zero pressure $GeSe_4$ was heated to 2000 K and kept there for 22 ps to lose the memory of initial positions. Subsequently, a number of different temperatures were visited before thermalizing the glassy structure at 300 K.[11] Three independent quenches with 1050 K being the starting temperature were performed in order to have a statistical average of the 300 K trajectories. The most energetically stable structures among the individual quenches were used to apply compression.

In order to apply pressure to the $GeSe_4$ structural model, the cell sizes were decreased under NVT conditions and the cell pressures were calculated from the average of the stress tensors over the useful parts of the trajectories (i.e., first 4 ps of 300 K trajectories were removed). We adopted a cold compression approach which signifies that the reduction of the cell volumes was performed at 300 K and pressure was successively increased using the last configurations of the subsequent trajectory.

We have simulated a certain number of thermodynamic data points (11) of amorphous $GeSe_4$. The former system is known to be isostatic ($n_c = 3$)[11] and located at the mean-field flexible/stressed rigid phase transition which is fulfilled when $n_c = 2 + 5x = 3$ or, alternatively, when the network mean coordination number $\bar{r} = 2 + 2x$ reaches the value of $\bar{r} = 2.4$. $GeSe_2$[11] is the stressed rigid (n_c = 3.67). The calculated residual pressure after melt quench is rather small (e.g., 0.35 GPa at 300 K for $GeSe_4$). A reduction (cold compression) of the cell size was then applied to increase the pressure up to 49.4 GPa (19.9 GPa for $GeSe_2$). The general methodology is the same as the one used for the recent investigations of a low pressurized $GeSe_4$ glass, and results are found to be comparable, while also agreeing with (i) thermal measurements and the equation of state[8,16] (see below) and (ii) the pair correlation $g(r)$ and the structure factor $S(k)$ obtained from neutron diffraction (ND) at low pressure (LP) (P < 14.4 GPa,[16]) and X-ray at higher pressures (HP),[8] as discussed in the following.

III. VALIDATION OF THE STRUCTURAL MODELS

Prior to the analysis of the effect of pressure on the rigidity of $GeSe_4$ glasses, we have indeed validated the reliability of our structural models of $GeSe_4$ by comparing our results with the available experimental data. A detailed comparison of our simulations to the experimentally measured quantities by neutron diffraction (ND) and x-ray diffraction (XRD) showed a good level of reproduction.

A. Reciprocal space properties

Figure 1 shows the AIMD calculated total structure factors for $GeSe_4$ during compression compared to neutron ($S_N(k)$) (Bouzid *et al.*[16]) and X-ray ($S_X(k)$) (Kalkan *et al.*[8]) diffraction experiments. The calculated structure factors show good agreement with experimental findings over the entire pressure range. One notices that the amorphous nature of the system is preserved until 49.2 GPa from the simulation results, in agreement with the experimental results shown for $Ge_{18}Se_{82}$ in our recent study,[17] indicating no crystallization up to 42 GPa. The typical ambient pressure features of the reciprocal space [the first sharp diffraction peak (FSDP) at k ∼ 1.15 $Å^{-1}$, the principal peak (PP) at k ∼ 2.05 $Å^{-1}$, and the secondary principal peak (PP2) at ∼3.62 $Å^{-1}$] are well reproduced along with the oscillation in higher k vectors (8–12 $Å^{-1}$) when compared to neutron diffraction results. The FSDP broadens and loses intensity as the pressure is increased and completely vanishes at around 7 GPa, as reported earlier for other chalcogenide systems under pressure.[16] Meanwhile the PP shifts to higher k values and a peak sharpening is observed which is coupled with an intensity increase. Similar observations can be made for the PP2. It is worth noting that the X-ray results show a more pronounced sharpening effect upon compression which was argued to be related to the higher resolution function used as compared to the neutron diffraction results

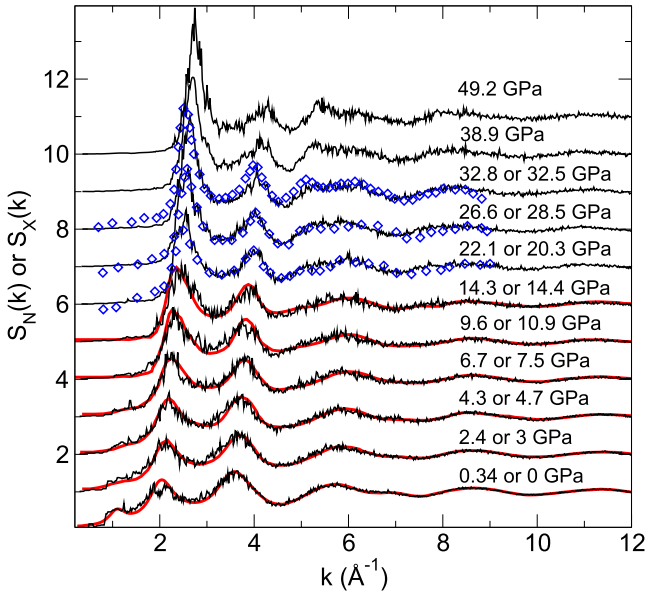

FIG. 1. Pressure dependence of the total structure factor $S(k)$ for $GeSe_4$. AIMD computed results (black curves) are compared to neutron diffraction (red curves)[16] and X-ray[8] diffraction (blue diamonds, digitized) results. Here, the first pressure value indicated corresponds to the simulations, while the second is for the experimental pressure points.

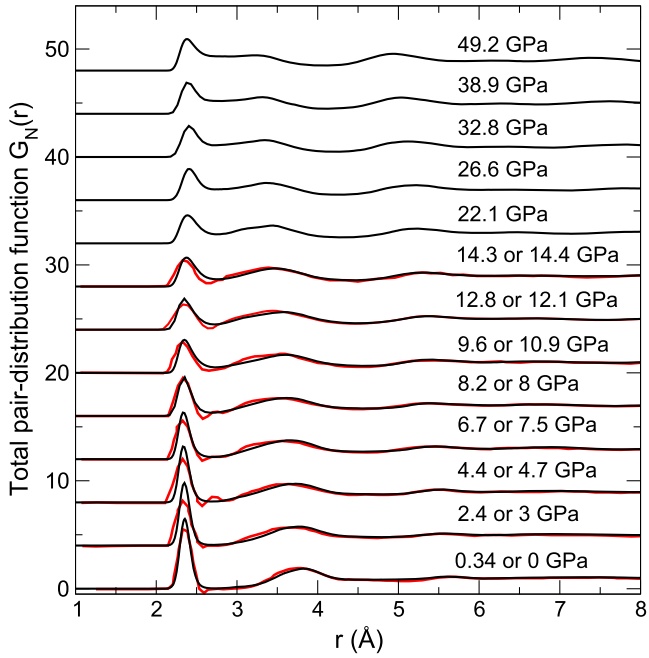

FIG. 2. Pressure dependence of computed (black curves) total pair distribution function for $GeSe_4$ is compared to neutron diffraction experiments[16] (red curves).

(Ref. 16 and the references therein). At higher pressures starting from 20 GPa, a peak located around k ~ 5 Å^{-1} builds up and becomes more pronounced as the pressure is increased. At pressures above 32 GPa, this peak is well separated from the PP2. The main contribution to the appearance of this peak is provided by the Se–Se partial structure factors, and also its feature is enhanced by the drop in the intensity of the Ge–Se partial structure factor around k ~ 4.6 Å^{-1} which are not shown here.

B. Real space properties

Turning to the real space properties, Fig. 2 shows the evolution of the computed total pair distribution function (PDF) $g(r)$ under pressure for $GeSe_4$ compared to ND results.[16] It appears that there is very good agreement between our simulations and the ND measurements at ambient pressure, as already acknowledged elsewhere.[16] The first peak located at ~2.36 Å and the second peak at ~3.85 Å are well reproduced. It should be noted that the intensity of the first peak at ambient pressure is slightly overestimated in simulations compared to the experiment. An overall agreement between ND and AIMD results can be observed for the pressure behavior of the PDF. Upon compression, the first peak loses intensity and shows a peak broadening. The position of this peak follows a similar trend with what is observed in Ge–Se bond length under pressure, as also shown experimentally.[17] The changes in this peak are directly reflected on the total coordination numbers (Fig. 3). The second peak continuously shifts to lower r values while losing its intensity along with a similar peak broadening.

Figure 4 shows the evolution of the partial PDF under pressure calculated with AIMD simulations. At ambient pressure, one notices absence of Ge–Ge homopolar bonds. This agrees with calculated coordination numbers (Fig. 3) where $\bar{n} = 2.4$ at ambient pressure with $\bar{n}_{Ge} = 4$ and $\bar{n}_{Se} = 2$, indicating predominant $Ge(Se_{1/2})_4$ units in the structure. The homopolar Ge–Ge bonds appear with increasing pressure, and the corresponding peak reaches a maximum intensity at around 15 GPa. Above this value, a decrease in the intensity is observed which is reflected to the Ge–Ge homopolar fraction. It can be seen that the peak corresponding to the Ge–Ge inter-atomic distance forming the edge-sharing (ES) tetrahedral connection (at around 3 Å) loses intensity and completely vanishes at

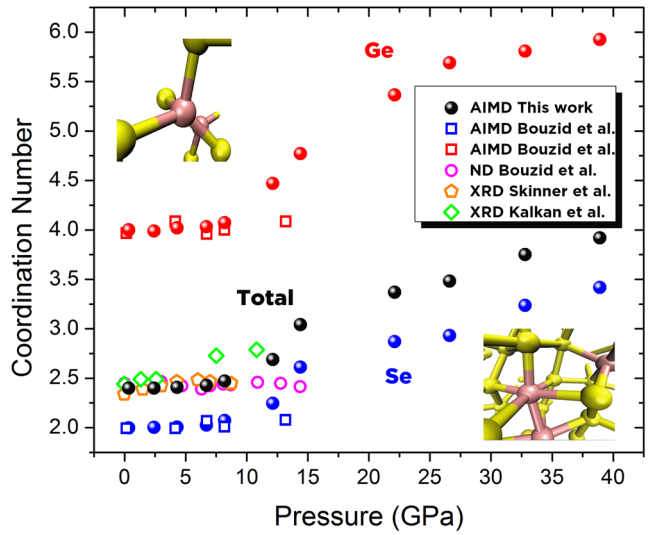

FIG. 3. Computed pressure dependence of computed coordination number $\bar{n}$ (black), $\bar{n}_{Ge}$ (red), and $\bar{n}_{Se}$ (blue) for $GeSe_4$ (filled spheres) is compared to the AIMD and ND work of Bouzid *et al.*[16] (open squares and magenta open circles, respectively), the XRD work of Skinner *et al.*[18] (orange open pentagons), and the XRD work of Kalkan *et al.*[8] (green open diamonds). On the top left and bottom right, snapshots of typical structural units are represented for LDA and HDA phases.

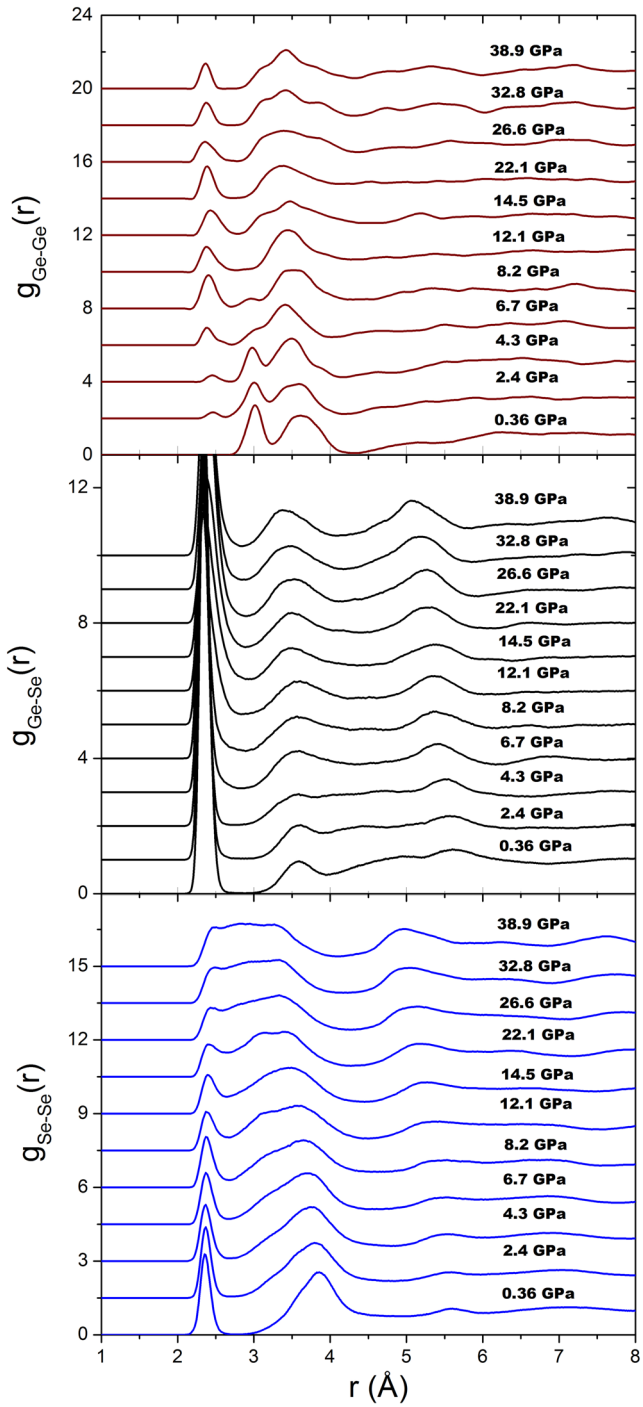

FIG. 4. The calculated pressure dependence of partial pair distribution functions for $GeSe_4$ [from upper panel to lower: $g_{GeGe}(r)$, $g_{GeSe}(r)$, and $g_{SeSe}(r)$].

12.1 GPa while the peak corresponding to corner-sharing (CS) tetrahedra broadens as the pressure is increased. Turning to $g_{GeSe}(r)$, one can notice that the position of the first peak located at ~2.35 Å behaves similar to what is observed for $Ge_{18}Se_{82}$ under pressure.[17] The second peak located at around ~3.66 Å at ambient pressure agrees well with the previous AIMD results,[11] which can be attributed to the distances of a cross-linking Ge atom with a Se chain. The intensity of this peak was reported to increase with increasing Ge content,[11] an indication that the increasing network connectivity yields an increase in the intensity of the secondary peak in $g_{GeSe}(r)$. Our simulations agree with a previous study[16] in the sense that for $P > 7$ GPa, the secondary peak gains intensity which is in line with the increased network rigidity. Finally, examining $g_{SeSe}(r)$ shows that the first peak associated with the homopolar Se–Se bonds is located at 2.36 Å, consistent with previous simulation[7,16] and diffraction work.[16] With increasing pressure, this peak loses intensity and broadens. The secondary peak that is located at 3.85 Å again shifts to smaller r values as the pressure is increased, eventually merging with the Se–Se homopolar peak at high pressure. This indicates that at high pressures, there is a high structural variety for the Se–Se type of bonding including motifs such as edge correlations of octahedral units, homopolar bonds, and connections with the next nearest neighbor as the fifth and sixth neighbors approaching the first shell.

Figure 3 shows the coordination numbers as a function of pressure for $GeSe_4$. Our AIMD results are compared to experimental and simulation studies available in the literature for this particular composition. The ambient pressure values for $\bar{n}$, $\bar{n}_{Ge}$, and $\bar{n}_{Se}$ are in line with the mean field calculations (i.e., $\bar{n} = 2 + 2x$, where x is the Ge mole fraction) and also consistent with previous contributions.[8,11,16] The rate of increase in coordination numbers is smaller at P > 22 GPa in such a way that $\bar{n}_{Ge}$ and $\bar{n}_{Se}$ almost linearly approach 6 and 4 at elevated pressures, respectively.

The slight discrepancies between the AIMD results in the work by Bouzid *et al.*[16] that an identical DFT scheme may be due to the different glass production prior to the cold compression in the simulations. Furthermore, there are differences in the total average coordination number $\bar{n}$ between XRD and ND measurements. The XRD work by Kalkan *et al.*[8] shows an increase in $\bar{n}$ at around $\sim P = 7.5$ GPa, reaching a similar value with our simulations at around 12 GPa while the coordination numbers found by ND measurements are almost constant up to $\sim P = 15$ GPa. It should be also noted that our simulation results shown in Fig. 3 are consistent with the work of Skinner *et al.*[18] indicating that there is no significant change in the coordination number at pressures up to 8.6 GPa.

C. Void structures

We extracted the total void volumes in $GeSe_4$ under pressure by calculating Voronoi volumes of each atom in our trajectories, similar to cavity characterizations.[19] The cut-off distances used as Voronoi parameters were taken from the minima of the first peak of the partial pair distribution function of the corresponding structure [e.g., at 4.2 GPa $g_{GeGe}(r)$ 2.69 Å, $g_{GeSe}(r)$ 2.73 Å, and $g_{SeSe}(r)$ 2.70 Å]. These analyses were carried out for the second half of the trajectories so that the void structures can become more stabilized after the dramatic squeezing effect of the exerted pressure at early times.

Figure 5 represents typical snapshots of $GeSe_4$ at different pressures with the void structure being represented in blue. Results indicate a rapid collapse of such voids given that for $P = 2.3$ GPa, the structure has densified to leave only minimal void fragments left. Such a void collapse manifests in $GeSe_2$ by the rapid conversion in the pressure

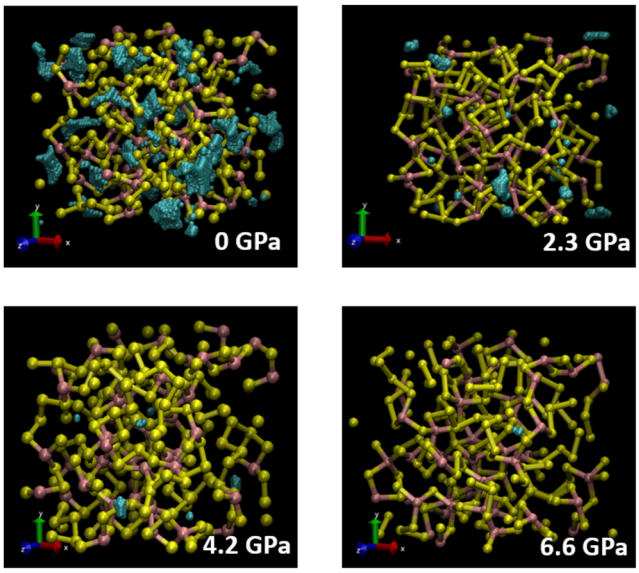

FIG. 5. Snapshots representing the change of the void structure (blue) at different pressures in $GeSe_4$. Note that voids completely disappear at 8.3 GPa.

range $0 \leq P \leq 3$ GPa of edge-sharing structures into corner-sharing tetrahedral connections,[20] an evolution that is compatible with the reduction of the amplitude of the ES peak in the present Ge–Ge pair correlation function (Fig. 4). Our corresponding void evolution can be tracked with pressure, as discussed below.

IV. EVIDENCE OF A LDA-HDA THRESHOLD

A certain number of calculated quantities exhibit a clear threshold located around $P_c = 10$ GPa, and this has been identified in the literature as the LDA-HDA transformation,[8] as also observed for other compositions (e.g., $Ge_{17}Se_{83}$, $P_c \simeq 15$ GPa[17]). The evolution of the calculated PP position of the total structure factor $S(k)$ of $GeSe_4$ (Fig. 1) is seen to be sensitive to the applied pressure [Fig. 6(a)] and reproduces the experimental trend measured at low P. The position of the PP increases, indeed, with pressure but clearly two different trends can be acknowledged, which indicate a rather fast increase of the PP position at low pressure (LP), i.e., a slope of 0.0267 $Å^{-1}$ Pa^{-1} followed by a somewhat more reduced evolution at higher pressure (HP), i.e., ≃0.0098 $Å^{-1}$ Pa^{-1} after 10 GPa. This change in slope, obviously, must indicate the existence of a pressure induced transformation for structural correlations in reciprocal space, whose location can be estimated at $P_c = 10.1$ GPa, i.e., quite close to the experimental estimate[8] (9.6 GPa). Following the work of Jeanloz,[21] the equation of state [the inset of Fig. 6(a)] can be linearized to yield a normalized stress $G = P/(3(1 + 2g)^{3/2})$ and an effective strain $g = \frac{1}{2}[(V_0/V)^{2/3} - 1]$ that are expressed as a function of the calculated pressure P and the volumes $V = V(P)$ and $V_0 = V(0)$. The corresponding behavior is shown in a $G(g)$ plot [Fig. 6(b)] that also indicates a transition point at ≃10 GPa which is found from the crossover between the high- and low-pressure behavior.

The advantage of such $G(g)$ plots is that a certain number of features of the transformation and the HDA phase

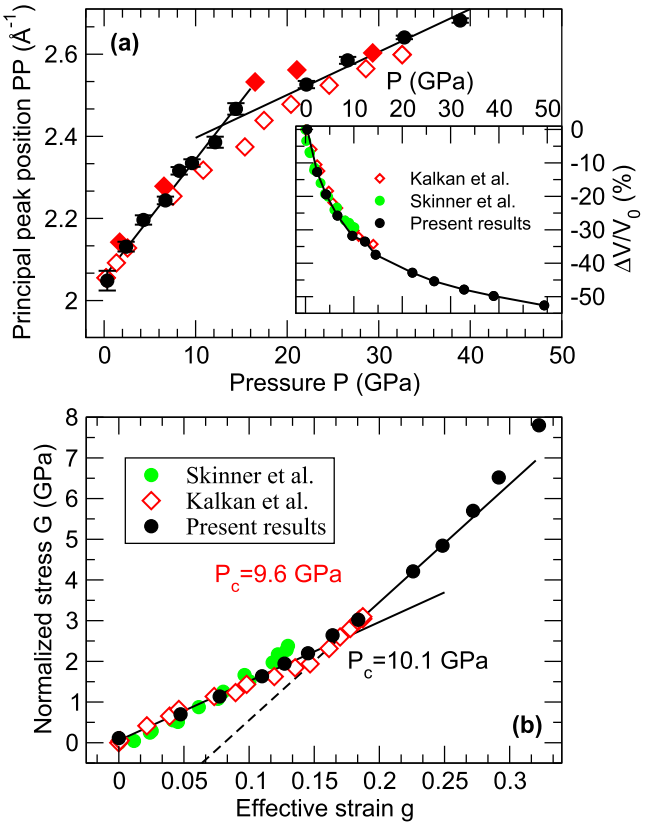

FIG. 6. (a) Principal peak (PP) position (filled circles) of the total structure factor $S(k)$ of $GeSe_4$ as a function of applied pressure P, compared to the results of Kalkan *et al.*[8] for compression (open red diamonds) and decompression (filled red diamonds). The inset shows the calculated equation of state $\Delta V/V_0$ of $GeSe_4$ that is compared to experimental measurements from Skinner *et al.*[18] and Kalkan *et al.*[8] (b) Calculated normalized stress G as a function of strain g (black filled circles), compared to experimental values (red open diamonds,[8] green circles[18]). The indicated pressures P_c correspond to the experimental (red) and theoretical (black) polyamorphic threshold pressures. Solid lines are linear fits to the results in the LDA and HDA phases.

can be characterized, the present MD simulations allowing also to go to much higher pressures (49.4 GPa) than the experimental ones (32 GPa[8]). First, the slope difference between the LP and HP behavior implies a discontinuity of the compressibility κ_T given that $dG/dg \propto (\kappa_T + P)$ with corresponding compressibilities equal to $0.10(4) \times 10^{-9}$ Pa and 0.005×10^{-9} Pa for the LDA and HDA phases, respectively. These values are rather consistent with those obtained experimentally; i.e., κ_T of the LDA phase has been found in the range $0.05–0.10 \times 10^{-9}$ Pa^{-1},[4,8,22] whereas the HDA compressibility has been determined to be of about 2 times smaller.[8] Second, the extrapolation of the HP behavior permits one to have a measure of the zero pressure volume of the HDA phase. By extrapolating the linear fits of the HP behavior to $G = 0$, we find a molar volume of $V/V_0 = 0.79(8)$ which is substantially smaller than the initial one characteristic of the LDA phase.

V. DISCUSSION

Our key result is that the observed transformation between a LDA and a HDA phase is linked with the features of rigidity, rigidity transitions, and topological constraints. This leads

to the emergence of a more complex picture which may not entirely be based on coordination changes with pressure.[2,5,9] To apply such an analysis to the densified $GeSe_4$, we have evaluated the density n_c of constraints per atom [Fig. 7(a)] between pairs or triplet of atoms, based from the MD atomic configurations. This enumeration is directly inspired by the classical mechanics view[25] of mechanical constraints associating large/small radial or angular motion with the absence/presence of corresponding bond-stretching (BS) and bond-bending (BB) restoring forces. In practice, one calculates the atomic radial and angular excursions around average values from the MD trajectories, and active topological constraints are then identified from their small radial and/or angular variances induced by the constraining interactions.[12,26,27] Previous applications on Ge_xSe_{1-x} glasses at $P = 0$[12] have shown that the mean field Phillips-Thorpe constraint count $n_c = 2 + 5x$[11] is exactly recovered for compositions ranging from $x = 0\%$ to 33% Ge, providing confidence that such calculations are accurate.

Here, it is found that for $GeSe_4$, n_c first remains constant with applied pressure and then starts to increase at a pressure (8.3 GPa) somewhat below P_c [Fig. 7(a)]. Given the isostatic and adaptive nature[28] of $GeSe_4$ at ambient conditions ($n_c \simeq 3$), the application of pressure does not modify the rigidity status in the range $0 < P < 8$ GPa, and n_c remains constant as long as voids or cavities are present in the structure [Fig. 7(a), right axis]. These voids tend to collapse

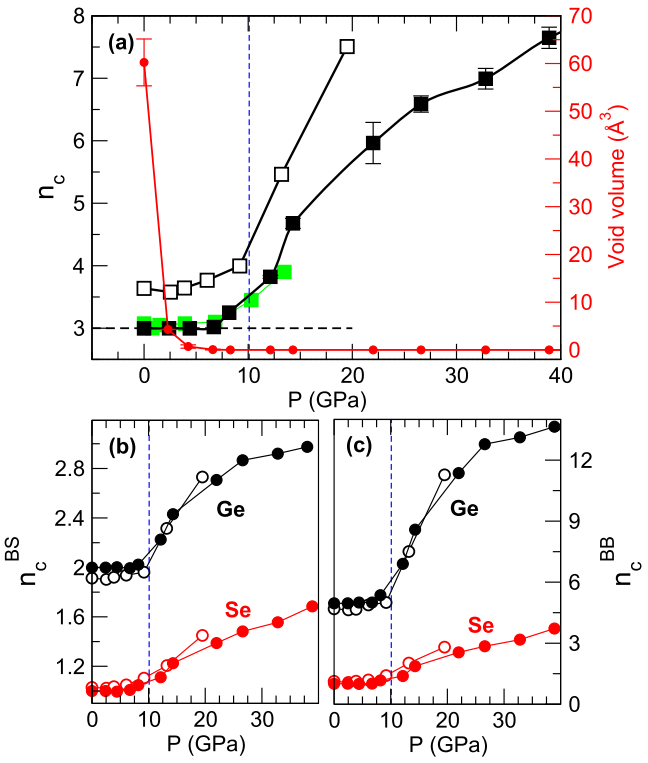

FIG. 7. (a) Calculated total number of constraints n_c as a function of pressure P for $GeSe_4$ (filled squares), $GeSe_2$ (open squares), and As_2Se_3 (green filled squares[23,24]). Right axis: Void volume (red curve) as a function of P. (b) Bond-stretching (BS) contribution of Ge (black) and Se (red) in $GeSe_4$ (filled symbols) and $GeSe_2$ (open symbols). (c) Corresponding bond-bending (BB) constraints. The LDA-HDA threshold pressure determined from Fig. 6 for $GeSe_4$ is signaled in all panels (blue broken line).

dramatically in the pressure range $0 < P < 6.6$ GPa (Fig. 7). Close to the LDA to HDA threshold however and because there are no more voids left to accommodate further densification, n_c now evolves rapidly with pressure to reach $n_c = 8.29$ for 49.2 GPa. This signals a network of extreme stiffness while also indicating a substantial growth of Ge and Se coordination numbers and, incidentally, BS and BB constraints. The obvious difference between the reduction of void at low pressure and the short-range evolution at larger pressure that also results in the constraint variation is actually compatible with results obtained for densified borosilicate glasses[29] which show that there is a decoupling between void collapse at low pressure and the short-range collapse at elevated pressures, a situation that is also met in pressurized zeolithes.[30,31]

A detailed analysis of the constraints [Figs. 7(b) and 7(c)] shows that the increase in rigidity is strongly driven by Ge atoms, and n_c^{BS} increases indeed to about 3 which can be associated with a nearly octahedral environment ($r_{Ge} = 2n_c^{BS} = 6$). This is linked with the usual picture of pressure-induced coordination increase given that n_c^{BS} scales as $r_i/2$ (i = Ge, Se). However, it is also reflected by the growth of the number of stiffer angles as shown from the **important** increase of n_c^{BB} for $P > 10$ GPa. Note that the transformation is also driven by the progressive loss of tetrahedral character which involves more and more p-bonded non-directional electronic states,[16] typical of an octahedral geometry and increased metallic character.[7] The location of the threshold P_c obtained from the evolution of the PP position and the stress-strain curve (Fig. 6) is, thus, found to be correlated with the pressure at which the isostatic nature of the network is lost ($n_c \neq 3$) and voids have collapsed.

These features actually induce a cascade of other important structural changes (Fig. 8). It is seen, indeed, that the bond statistics also evolves when moving from the LDA to the HDA phase, the former being characterized by a rather important fraction of Ge–Se (67%) bonds (see also Ref. 11), whereas the latter contains a substantially reduced population (55%). Note that the fraction of Ge–Ge bonds never exceeds 2.0% given the Ge-deficient stoichiometry of $GeSe_4$.[11] Conversely, the population of Se–Se bonds grows substantially over the same pressure interval and leads to a nearly constant value of 45% for $P > 22$ GPa. The HDA phase, furthermore, shows a continuous distribution of Se–Se correlations between 2.2 and 3.4 Å, a quite unusual feature which signals that the Se-related structuration of the glass made of a well-defined first and second neighbouring shell at ambient conditions has been completely lost. The partial pair correlation function $g_{SeSe}(r)$ displays, indeed, a nearly constant (plateau) value for $r < 3.4$ Å (Fig. 4), indicative of a variety of structural motifs and chemical bondings (atomic configuration, Fig. 8): edge correlations on a $GeSe_{6/2}$ octahedra (≃3.1 Å), homopolar Se–Se bondings (2.4–2.6 Å), correlations between the octahedra vertex, and the next-nearest neighbours that become very close due to the pressure induced buckling of the structure (2.7–3.0 Å). All these observations lead to the conclusion that a pressure induced stressed rigid transition parallels the LDA-HDA transformation, as $n_c > 3$.

A natural question that emerges at this stage is the degree of generality of these results for other compositions,

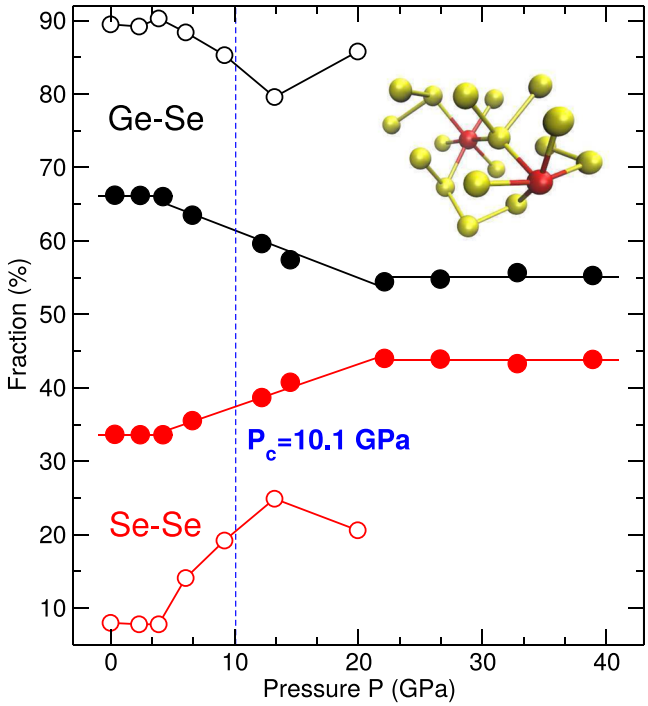

FIG. 8. Calculated fraction of Ge–Se and Se–Se bonds in $GeSe_4$ (filled symbols) and $GeSe_2$ (open symbols) as a function of pressure. A cut-off distance of 2.8 Å has been used (minimum of the total pair correlation function). On the top is represented a typical fragment of the HDA atomic structure at 39 GPa in $GeSe_4$.

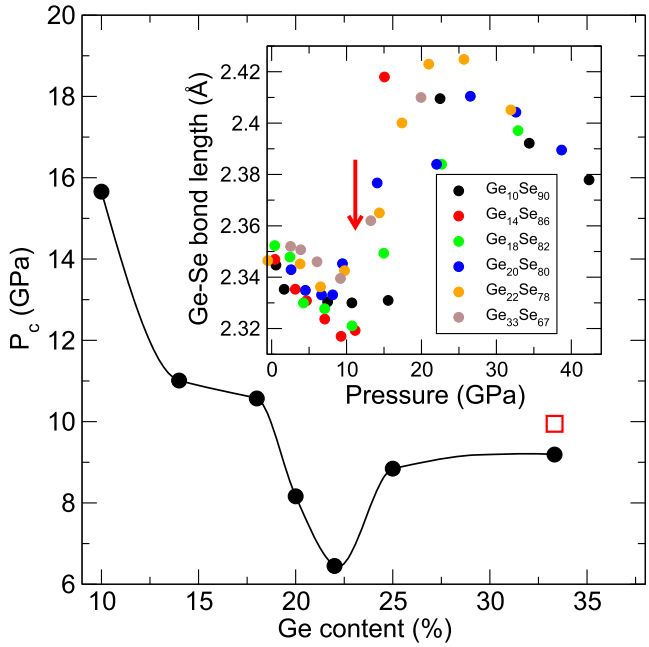

FIG. 9. LDA-HDA transition pressure P_c as a function of Ge content x in Ge_xSe_{1-x} glasses, determined from the pressure evolution of simulated Ge–Se bond distances at select compositions (the inset of Ref. 17). The pressure P_c has been chosen at the bond distance value closest to the marked jump (arrow for, e.g., $Ge_{14}Se_{86}$). The open red square corresponds to an experimental data point from Properzi *et al.*[32]

and, particularly, how the LDA-HDA transformation behaves with the Ge content x in Ge_xSe_{1-x} that covers the flexible, the intermediate, and the stressed rigid phase.[11] The same analysis performed on the stressed rigid $GeSe_2$ shows that the detailed constraint count leads to an identical trend with pressure [Figs. 7(b) and 7(c)] and a threshold pressure $P_c \simeq 10$ GPa, consistently with Ref. 32, whereas the total $n_c(P)$ is only shifted by a value $n_c(0) - 3 = 0.67$ due to the increased concentration of Ge atoms [Fig. 7(a)]. These results are also consistent with densified As_2Se_3 (green symbols) which is isostatic[23] at zero pressure, and a nearly perfect overlap with the isostatic $GeSe_4$ result is obtained across the LDA-HDA transition. Similarly, the strong increase obtained for the constraint density across the threshold P_c for $GeSe_2$ is found parallel to the important changes in bonding population. In fact, Fig. 8 indicates that the fraction of Ge–Se and Se–Se bonds in $GeSe_2$ also undergo a rapid change as P increases.

An account of coupled effects on pressure-induced amorphous phases and rigidity can now be sketched. Previous numerical and experimental investigation of a series of compositions in moderately densified Ge–Se glasses[17] show that under pressure the Ge–Se bond distance first reduces prior to an important increase at the LDA-HDA threshold located at $P = P_c$, resulting in a typical elongation of about 0.09 Å. These numerical trends (the inset of Fig. 9) are globally consistent with x-ray absorption spectroscopy[17] and neutron diffraction.[16] The pressure P_c at which this abrupt change occurs obviously depends on the composition, and when represented as a function of Ge content (Fig. 9), one realizes that P_c does not evolve monotonically and contains an anomaly that reveals fingerprints of the underlying rigidity status of the network[11] (flexible, intermediate, stressed). In both the chalcogen-rich flexible and the Ge-rich stressed rigid domains (e.g., $Ge_{10}Se_{90}$ and $Ge_{33}Se_{67}$, respectively), glasses are characterized by rather large molar volumes,[34] larger bulk moduli,[33] and reduced elastic recovery under load.[35] There is, therefore, the need of larger pressures in order to switch from LDA to HDA and induce coordination changes because there is also available free volume, a situation that is particularly met for weakly cross-linked selenium chains (e.g., $Ge_{10}Se_{90}$). On the contrary, for Ge–Se glasses that belong to the so-called Boolchand intermediate phase (20%–25% Ge), it is well known that the absence of stress (isostaticity) leads to space-filling tendencies,[36] and, in fact, the molar volume is minimum between 20% and 25% Ge,[34] as also recently found in the As–Se binary.[37] Sensitivity to polyamorphism is, thus, enhanced for glasses with a higher density, and P_c is shifted to lower pressures for such almost isostatic compositions having also a reduced relaxation kinetics[37,38] due to their strong glass-forming character. A similar sensitivity to pressure has been acknowledged for intermediate Ge–Se compositions in Raman studies.[28] One might, therefore, expect to have LDA-HDA transformations at lower pressures for glasses displaying space-filling tendencies as in $AsSe_3$[37] or $Ge_8Si_8Te_{84}$.[39]

VI. CONCLUSION

Here, we have used AIMD simulations to investigate the pressure effect of amorphous $GeSe_4$, a material of fundamental interest given its particular isostatic nature, at the edge of flexible to rigid transitions. With pressure, a signature of a LDA to HDA threshold is detected from structural changes and from stress-strain representations. The substantial increase of the

constraint density appears to occur in the same pressure range as the LDA-HDA transformation.

Given that both LDA-HDA transformations and flexible to rigid transitions are found in a variety of glassy materials and given that pressure-induced rigidity is one efficient numerical alternative to stiffen network structures,[12] it would be certainly of great interest to investigate other potential model systems in order to contrast such transitions in other typical chalcogenides with changing connectedness (e.g., Ge_xS_{1-x}). Similarly, there are a certain number of archetypal isostatic compounds (GeS_4, SiO_2, As_2S_3, ...) that may well be investigated experimentally both from the viewpoint of rigidity and polyamorphism. Finally, it is also well known that molecular systems can undergo LDA-HDA transformations as exemplified by metal-organic glasses[40] or amorphous water,[3] this transformation being now also observed in mesoporous materials[31] which associate the pressure-driven void collapse with a non-trivial decelerated melting kinetics. A neat definition of network connectedness might be particularly difficult to establish for certain of these systems but it is important to emphasize that the MD based constraint count has a general basis and can here be applied as well.[27] A direct application of such methods to structural models of amorphous water[41] leads to $n_c = 1.67$ at ambient pressure and to $n_c = 3.67$ at 0.5 GPa, the LDA-HDA transition being approximatively found at 0.2 GPa;[3] i.e., flexible water at $P = 0$ becomes stressed rigid as pressure is applied. In this context, recent attempts[42] to capture the effects of weak (van der Waals) interactions on the relationship between rigidity and physico-chemical properties might be particularly helpful, and, e.g., shell models of amorphous water appear to be attractive systems to further decode coupled effects of rigidity and polyamorphism.

ACKNOWLEDGMENTS

C.Y. acknowledges IDS FunMat (Project No. 2013-05-EM) and Onderzoeks Centrum voor de Aanwending van Staal (OCAS) for the financial support of his Ph.D. and post-doctoral projects, respectively. C.Y. and J.Y.R. gratefully acknowledge the computational resources provided by the Consortium des Équipements de Calcul Intensif (CÉCI), funded by the Fonds de la Recherche Scientifique de Belgique (F.R.S.-FNRS) under Grant No. 2.5020.11, and the Tier-1 supercomputer of the Fédération Wallonie-Bruxelles, infrastructure funded by the Walloon Region under the Grant Agreement No. 1117545. M.M. acknowlegdes computational resources from Plateforme Romeo de l'Université de Reims Champagne-Ardenne.

[1] P. H. Poole, Science **275**, 322 (1997).
[2] A. C. Barnes, L. B. Skinner, P. S. Salmon, and A. Bytchkov, Phys. Rev. Lett. **103**, 225702 (2009).
[3] O. Mishima, L. Calvert, and E. Whalley, Nature **314**, 76 (1985).
[4] L. B. Skinner, A. C. Barnes, P. S. Salmon, and W. A. Crichton, J. Phys.: Condens. Matter **20**, 205103 (2008).
[5] A. Zeidler *et al.*, Phys. Rev. Lett. **113**, 135501 (2014).
[6] F. Pacaud and M. Micoulaut, J. Chem. Phys. **143**, 064502 (2015).
[7] M. Durandurdu and D. A. Drabold, Phys. Rev. B **65**, 104208 (2002).
[8] B. Kalkan, R. P. Dias, C.-S. Yoo, S. M. Clark, and S. Sen, J. Phys. Chem. C **118**, 5110 (2014).
[9] K. Wezka, A. Bouzid, K. J. Pizzey, P. S. Salmon, A. Zeidler, S. Klotz, H. E. Fischer, C. L. Bull, M. G. Tucker, M. Boero, S. Le Roux, C. Tugène, and C. Massobrio, Phys. Rev. B **90**, 054206 (2014).
[10] V. V. Brazhkin, E. Bychkov, and O. B. Tsiok, J. Phys. Chem. B **120**, 358 (2016).
[11] M. Micoulaut, A. Kachmar, M. Bauchy, S. Le Roux, and C. Massobrio, Phys. Rev. B **88**, 054203 (2013).
[12] C. Yildirim, J.-Y. Raty, and M. Micoulaut, Nat. Commun. **7**, 11086 (2016).
[13] K. Trachenko, M. T. Dove, V. Brazhkin, and F. S. El'kin, Phys. Rev. Lett. **93**, 135502 (2004).
[14] S. Bhosle, K. Gunasekera, P. Boolchand, and M. Micoulaut, Int. J. Appl. Glass Sci. **3**, 205 (2012).
[15] J. Ruska and H. Thurn, J. Non-Cryst. Solids **22**, 277 (1976).
[16] A. Bouzid, K. Pizzey, A. Zeidler, G. Ori, M. Boero, C. Massobrio, S. Klotz, H. Fischer, C. L. Bull, and P. S. Salmon, Phys. Rev. B **93**, 014202 (2016).
[17] C. Yildirim, M. Micoulaut, P. Boolchand, I. Kantor, O. Mathon, J.-P. Gaspard, T. Irifune, and J.-Y. Raty, Sci. Rep. **6**, 27317 (2016).
[18] L. B. Skinner, C. J. Benmore, S. Antao, E. Soignard, S. A. Amin, E. Bychkov, E. Rissi, J. B. Parise, and J. L. Yarger, J. Phys. Chem. C **116**, 2212 (2011).
[19] J. Akola and R. O. Jones, Phys. Rev. Lett. **100**, 205502 (2008).
[20] S. M. Antao, C. J. Benmore, B. Li, L. Wang, E. Bychkov, and J. B. Parise, Phys. Rev. Lett. **100**, 115501 (2008).
[21] R. Jeanloz, Geophys. Res. Lett. **8**, 1219, https://doi.org/10.1029/gl008i012p01219 (1981).
[22] J. P. Guin, T. Rouxel, J. C. Sangleboeuf, I. Melscoët, and J. Lucas, J. Am. Ceram. Soc. **85**, 1545 (2002).
[23] M. Bauchy, A. Kachmar, and M. Micoulaut, J. Chem. Phys. **141**, 194506 (2014).
[24] M. Micoulaut, unpublished results.
[25] F. Wilcek, Phys. Today **57**(10), 11 (2004).
[26] M. Bauchy and M. Micoulaut, J. Non-Cryst. Solids **377**, 34 (2013).
[27] M. Bauchy and M. Micoulaut, Phys. Rev. Lett. **110**, 095501 (2013).
[28] F. Wang, S. Mamedov, P. Boolchand, B. Goodman, and M. Chandrasekhar, Phys. Rev. B **71**, 174201 (2005).
[29] B. Mantisi, S. Adichtchev, S. Sirotkin, L. Rafaelly, L. Wondraczek, H. Behrens, C. Marcenat, N. V. Surovtsev, A. Pillonnet, and E. Duval, J. Phys.: Condens. Matter **22**, 025402 (2010).
[30] J. Haines, C. Levelut, A. Isambert, P. Hébert, S. Kohara, D. A. Keen, T. Hammouda, and D. Andrault, J. Am. Chem. Soc. **131**, 12333 (2009).
[31] L. Wondraczek, Z. Pan, T. Palenta, A. Erlebach, S. T. Misture, M. Sierka, M. Micoulaut, U. Hoppe, J. Deubener, and G. N. Greaves, Adv. Sci. **5**, 1700850 (2018).
[32] L. Properzi, A. Di Cicco, L. Nataf, F. Baudelet, and T. Irifune, Sci. Rep. **5**, 11088 (2015).
[33] V. V. Brazhkin, E. Bychkov, and O. B. Tsiok, J. Exp. Theor. Phys. **123**, 308 (2016).
[34] S. Bhosle, P. Boolchand, M. Micoulaut, and C. Massobrio, Solid State Commun. **151**, 1851 (2011).
[35] J. C. Mauro and A. K. Varshneya, J. Am. Ceram. Soc. **90**, 192 (2007).
[36] C. Bourgel, M. Micoulaut, M. Malki, and P. Simon, Phys. Rev. B **79**, 024201 (2009).
[37] S. Ravindren, K. Gunasekera, Z. Tucker, A. Diebold, P. Boolchand, and M. Micoulaut, J. Chem. Phys. **140**, 134501 (2014).
[38] K. Gunasekara, S. Bhosle, P. Boolchand, and M. Micoulaut, J. Chem. Phys. **139**, 164511 (2013).
[39] K. Gunasekera, P. Boolchand, and M. Micoulaut, J. Appl. Phys. **115**, 164905 (2014).
[40] T. D. Bennett *et al.*, Nat. Commun. **6**, 8079 (2015).
[41] N. Giovambattista, C. A. Angell, F. Sciortino, and H. E. Stanley, Phys. Rev. Lett. **93**, 047801 (2004).
[42] L. Yan and M. Wyart, Phys. Rev. Lett. **113**, 215504 (2014).